


## Correlated disorder as a way towards robust superconductivity

Vyacheslav D. Neverov<sup>1,2</sup>, Alexander E. Lukyanov<sup>1,2</sup>, Andrey V. Krasavin<sup>1,2</sup>  <sup>✉</sup>, Alexei Vagov<sup>2,3</sup> & Mihail D. Croitoru<sup>2,4</sup>

Ordinary superconductors are widely assumed insensitive to small concentrations of random nonmagnetic impurities, whereas strong disorder suppresses superconductivity and even makes superconductor-insulator transition occur. In between these limiting cases, a most fascinating regime can take place where disorder enhances superconductivity. Hitherto, almost all theoretical studies have been conducted under the assumption that disorder is completely independent and random. In real materials, however, positions of impurities and defects tend to correlate with each other. This work shows that these correlations have a strong impact on superconductivity making it more robust and less sensitive to the disorder potential. Superconducting properties can therefore be controlled not only by the overall density of impurities and defects, but by their spatial correlations as well.

<sup>1</sup>National Research Nuclear University MEPhI, Moscow, Russian Federation. <sup>2</sup>HSE University, Moscow, Russian Federation. <sup>3</sup>Institut of Theoretical Physics Physics III, University of Bayreuth, Bayreuth, Germany. <sup>4</sup>Departamento de Física, Universidade Federal de Pernambuco, Recife-PE, Brazil.  
✉email: [avkrasavin@mephi.ru](mailto:avkrasavin@mephi.ru)

Founding theoretical studies of Abrikosov and Gorkov<sup>1</sup> of superconductivity in a disordered material were followed up by a general physical consideration by Anderson<sup>2</sup> according to which superconductivity with the  $s$  pairing symmetry is insensitive to weak nonmagnetic disorder. Subsequent experimental studies, however, demonstrated that superconductivity is suppressed in strongly disordered samples. A very strong disorder can lead to a metal–insulator transition in the normal state, to the appearance of a pseudogap in spectrum, to larger spatial fluctuations of superconductive pairing, and increased  $\Delta/T_c$  ratio<sup>3–10</sup>. Theoretical investigations have largely supported the experimental results<sup>11–13</sup>.

The recent advent of the quasi-2D materials era has opened up new horizons in physics of disordered systems including superconductors. Many phenomena important for electrical transport, such as renormalization of the electron–electron interactions, Anderson localization, and phase fluctuations, are boosted in low-dimensional structures, resulting in suppression of superconductivity. The detrimental effects of lowered dimension in combination with disorder were observed in amorphous as well as highly crystalline 2D superconductors<sup>14–19</sup>.

The disorder can also result in a remarkable enhancement in superconductivity figures of merit. The disorder potential controls the interplay between the superconductive pairing and long-range phase coherence. The stronger disorder increases spatial inhomogeneity, which enhances the local pairing correlations and superconducting gap, comparing with the clean system<sup>20</sup>. Recent studies have revealed an unprecedented disorder-induced increase in the superconductivity pairing instability in quasi-1D single crystals made of MoSe chains weakly bound by Na atoms<sup>21</sup>. An anomalous superconductivity enhancement due to large structural disorder was also reported for TaS<sub>2</sub> monolayers<sup>22</sup>. Disorder-related effects are assumed responsible for a large increase of the critical temperature in the recently discovered superconducting NbSe<sub>2</sub> monolayers<sup>23</sup>. Theoretical analysis attributes the enhancement to the disorder-induced *multi-fractal* structure of the electronic wave functions<sup>24,25</sup>, which was observed by numerically solving microscopic theory equations in low-dimensional samples<sup>26</sup>. The calculations predict the cluster formation and survival of the spectral gap even at extremely large disorder<sup>27</sup>.

On the other side, strong disorder enhances phase fluctuations, thereby reducing the superfluid density (stiffness), and suppressing superconductivity on the global scale. With the changing disorder strength the system can, therefore, have an optimal degree of inhomogeneity, where the superconductivity enhancement and the critical temperature  $T_c$  are maximal<sup>28</sup>. Notice, that a similar mechanism underlies superconductivity enhancement in samples where inhomogeneities are related to the quantum size effects<sup>29–31</sup>.

Introducing random impurities and defects in otherwise ordered materials can thus be regarded as a tool to control superconducting characteristics of materials, a design element to engineer superconductors with desired functionalities. However, one of the main problem with this approach is to identify key parameters of the impurity distribution which affect the superconductive state. Solving it requires detailed numerical simulations that account for the disorder distribution in real materials.

Most theoretical investigations of disordered superconductors are based on the models with the spatially uncorrelated disorder, which are analyzed using the perturbation expansion methods. In real systems, however, the disorder is almost never completely random. The inhomogeneities are often arranged in a certain structure, characterized by the long-range spatial correlations. There is a growing appreciation of the fact that such correlations can change essential properties of disordered systems qualitatively<sup>32–34</sup>.

Prominent examples of this type include opening resonant transmission channels<sup>35</sup>, modifying metal–insulator transitions<sup>36</sup>, and changing mobility edges<sup>37</sup>. Effects related to the disorder correlations have been experimentally observed in gases of cold atoms<sup>38,39</sup> and photonic systems<sup>40</sup>. Also, correlated deviations from the ideal periodicity of a crystal structure plays a significant role for functional materials<sup>41</sup> that utilize ionic conductivity<sup>42</sup> and their ferroelectric<sup>43,44</sup>, thermoelectric<sup>45</sup>, and photoelectric properties<sup>46</sup>. Achieving desired functionalities by manipulating patterns of the structural disorder is one of the goals of contemporary material science studying disordered crystals<sup>33,47</sup>.

In recent experiments with dirty superconducting films<sup>23</sup>, a visual analysis of the disorder distribution reveals spatial long-range correlations. It is clear, the superconducting state will be much more complex when the disorder is spatially correlated. The correlations introduce an additional characteristic length-scale that competes with those defined by the BCS coherence length  $\xi$  and the Fermi wave length  $\lambda_F$ . It has been previously shown that superconductivity can be strongly boosted in both of the opposite limiting cases: when the external potential is fully random and uncorrelated<sup>26,27</sup>, and when it has a fixed ordered structure without the random component<sup>20,48,49</sup>. However, very little if anything is known about a most relevant situation, where an inherently random distribution of material inhomogeneities acquires a certain degree of spatial correlations. The goal of this work is to initiate studies of an interplay of “order and disorder” in superconductors, with a strategic goal to find the optimal balance for the most robust superconducting state.

Here, we investigate the influence of the long-range correlations of the disorder potential on the superconducting state at zero temperature. The analysis is done by calculating superconducting properties of 2D sample using a disordered model with spatial correlations. Our analysis shows that long-range correlations can considerably change statistical properties of the Cooper pairing and enhance multi-fractal features of the order parameter. As the result, global superconductivity becomes more robust with respect to the disorder strength.

## Results and discussion

The calculations are done using the model of the structural disorder where the spatial correlations of the disorder potential in the inverse space obey the power law

$$S_V(q) \propto q^{-\alpha} \quad (1)$$

in the limit of small  $q$ . The power exponent  $\alpha$  determines the *correlation degree*. When  $\alpha = 0$  the random potential  $V_i$  at different lattice sites is fully uncorrelated. The spatial correlations of the random potential in the real space are characterized by the correlation length  $\xi_V$  calculated in the Methods section.

**Spatial profile of the disorder.** We start the analysis with showing in the row (a) of Fig. 1 typical spatial profiles of a disorder potential  $V_i$  obtained for different values of the correlation degree  $\alpha = 0, 1, 2, 3$ . For the fully uncorrelated disorder with  $\alpha = 0$  the color density plot representation for the profile appears as fully randomly distributed array of “pixels” or grains. When  $\alpha$  increases the pixels are smoothed out gradually forming textures or structures of larger dimensions, on the scale  $\xi_V$  (see Fig. 2a). It is to be noted that positions, shapes and orientation of those textures are still random, such that the ensemble-averaged system remains homogeneous (if the number of disorder realization is large enough).

**Spatial profile of the order parameter.** Using the above configurations of the disorder potential we solve the Bogoliubov – de

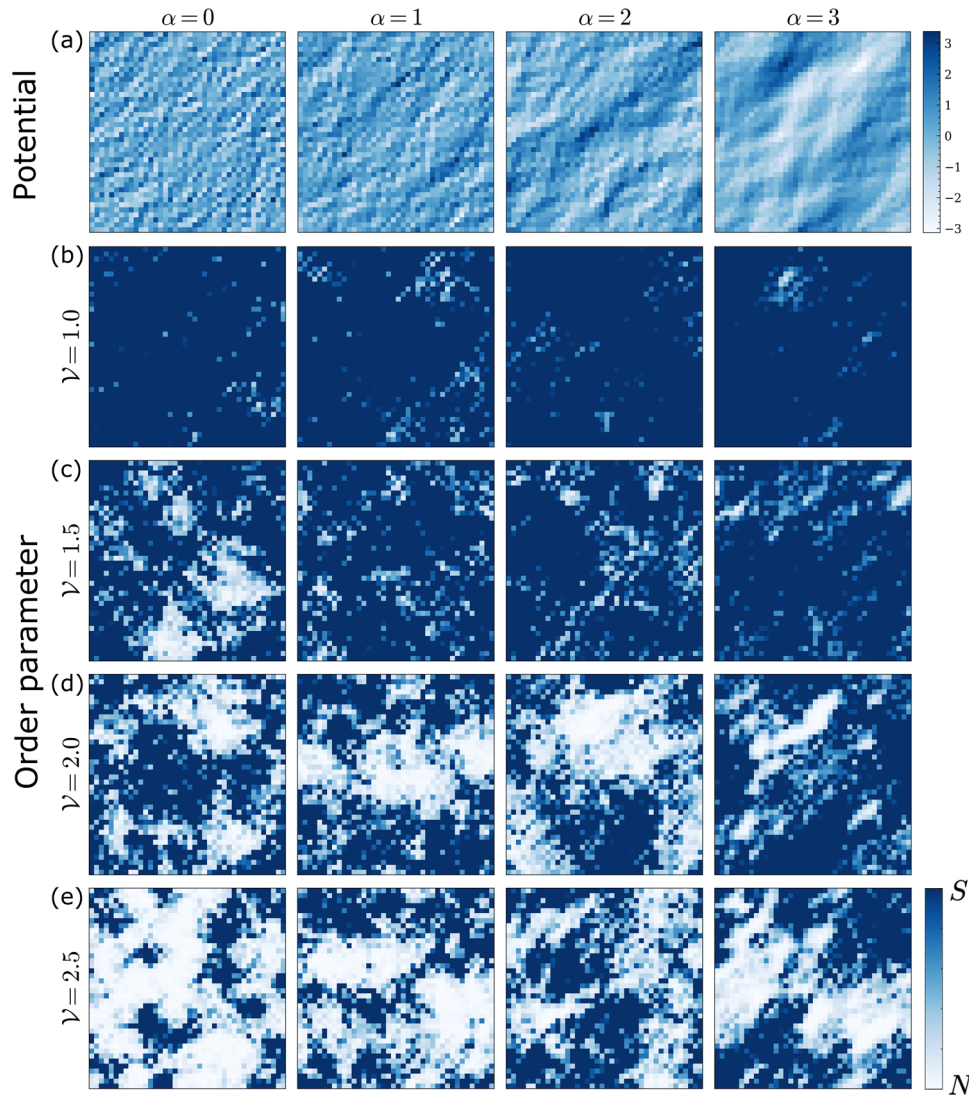


**Fig. 1 Spatial profiles of disorder potential and order parameter.** Color density plot of the spatial profile of the random potential  $V_i$  (row a) and of the order parameter  $\Delta_i$  (rows b–e), calculated assuming the disorder strength of  $\nu = 1.0, 1.5, 2.0, 2.5$  and the disorder correlation degree  $\alpha = 0, 1, 2, 3$  (panel columns). Blue and white colors denote, respectively, superconducting  $S$  and normal  $N$  domains. Each panel has its own scaling chosen for a better contrast and visibility of the regions with weak superconductivity: dark blue corresponds to the gap value  $\Delta_i > 0.1\bar{\Delta}_i$ , where  $\bar{\Delta}_i$  is the average gap value.

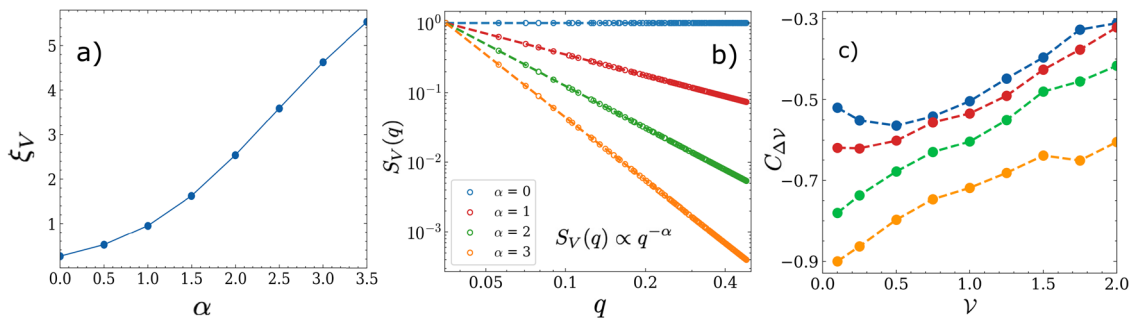


**Fig. 2 Correlation properties of random potential.** **a** The dependence of the correlation length  $\xi_V$  for the random potential model in Eq. (16) on the correlation degree  $\alpha$ . **b** the Fourier transform  $S_V(q)$  of the spatial correlation function of the random potential, given for selected values of  $\alpha$ . **c** the integral degree of correlations between the disorder potential  $V_i$  and the order parameter  $\Delta_i$ , defined in Eq. (2), as function of the disorder strength  $\nu$ , given for several values of the potential correlation degree  $\alpha$ .

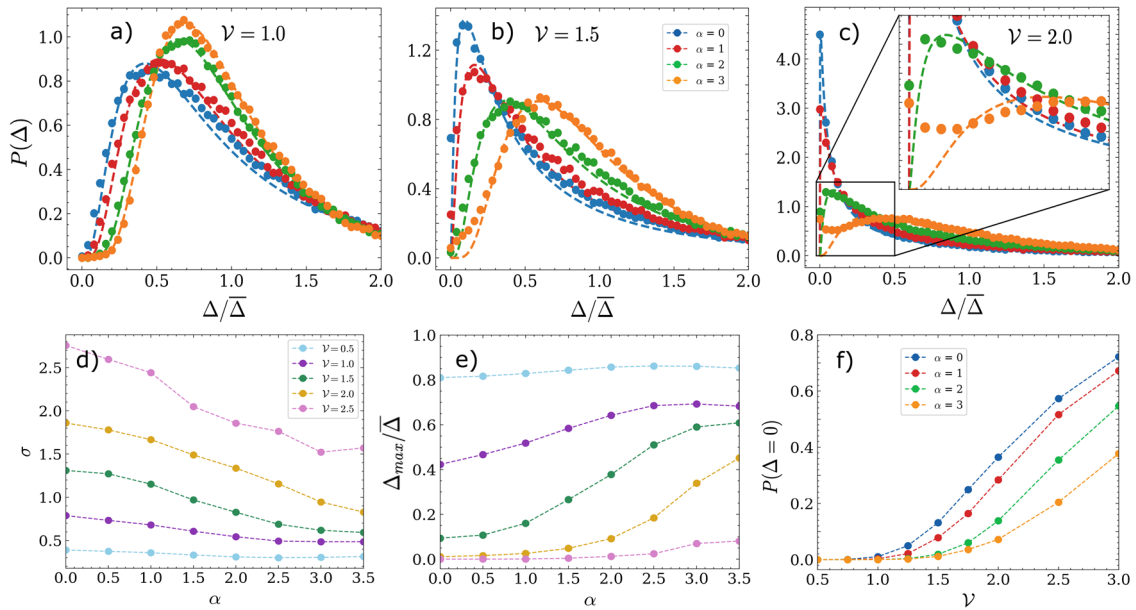


**Fig. 3 Statistical properties of the order parameter.** Statistical distribution  $P(\Delta)$  of the absolute value  $\Delta$  of the order parameter, relative to its sample and disorder averaged value  $\bar{\Delta}$ , calculated at  $\mathcal{V} = 1.0$  (a),  $\mathcal{V} = 1.5$  (b),  $\mathcal{V} = 2.0$  (c), for a few selected values of  $\alpha$ . The dashed lines give the best fit of the obtained numerical data using the normal-log distribution in Eq. (3). **d, e** give the  $\alpha$  dependence of the distribution width  $\sigma$  and its peak position  $\Delta_0$ , obtained in the fit. **f** is the probability of zero gap  $P(\Delta \simeq 0)$  ( $0 < \Delta < 0.1\bar{\Delta}$ ) as a function of  $\mathcal{V}$ . The dashed lines, connecting numerically obtained points in the lower panels, are guides for an eye.

Genes (BdG) equations and obtain the order parameter profile. The results for different values of the disorder strength  $\mathcal{V} = 1, 1.5, 2, 2.5$  are shown in the rows (b–e) in Fig. 1, where columns correspond to the selected values of  $\alpha$ . The blue color indicates domains of the superconductive phase of  $\Delta_i \neq 0$  and the white color marks domains of the normal phase with  $\Delta_i \simeq 0$ . The deep blue color indicates  $\Delta_i > 0.1\bar{\Delta}_i$ , where  $\bar{\Delta}_i$  is the full-ensemble and lattice average of the order parameter. Note, that each panel in the plot has its own scaling for a better contrast, to highlight details of domains of weak superconductivity.

First, we consider the case of uncorrelated disorder investigated extensively in earlier works<sup>11,12,27</sup>. It is well known that when the disorder is weak the disorder parameter is homogeneous. This trivial case is not shown in Fig. 1. However, the panel obtained at relatively small strength  $\mathcal{V} = 1$  and  $\alpha = 0$  demonstrates that the order parameter is close to being homogeneous, and the normal phase occurs only in a restricted number of small-size domains.

When the strength  $\mathcal{V}$  increases, the superconducting state becomes inhomogeneous. Blue superconducting (S) clusters with larger values of the order parameter are mixed with white normal state (N) regions. The clustering in the order parameter profile appears not strongly correlated with the disorder potential: one sees in Fig. 1 that the disorder profile at  $\alpha = 0$  shows no textures with sizes comparable to clusters of order parameter  $\mathcal{V} > 1$ . The clustering is a manifestation of the multi-fractal properties of the BdG solutions. The degree of correlations between the potential and the order parameter can be described by the statistical correlator

$$C_{\Delta\mathcal{V}} = \frac{|\overline{\Delta_i \mathcal{V}_i} - \overline{\Delta_i} \overline{\mathcal{V}_i}|}{\sigma_{\Delta} \mathcal{V}}, \quad \sigma_{\Delta} = \sqrt{|\overline{\Delta_i^2} - \overline{\Delta_i}|^2} \quad (2)$$

where  $\mathcal{V}_i = |V_i + U_i - \mu_i|$ , and which characterizes the suppression of superconductivity by the random potential. Results for the calculations are shown in Fig. 2c. At  $\alpha = 0$  and  $\mathcal{V} = 1$  one obtains  $C_{\Delta\mathcal{V}} \simeq -0.5$  which corresponds to a relatively weak negative correlation between the gap  $\Delta_i$  and potential  $V_i$ .

The order parameter profile, shown in Fig. 1 for  $\alpha \neq 0$ , demonstrates how it changes with the disorder potential strength  $\mathcal{V}$  and the correlation degree  $\alpha$ . First, one notes that the order parameter becomes more homogeneous at larger  $\alpha$ : sizes of normal clusters decrease making the system “more superconductive”. At large values of  $\alpha$ , a typical size of the order parameter cluster (N or S) is comparable to that of textures of the disorder potential. This implies the order parameter and disorder potential become more correlated, which is demonstrated in Fig. 2c.

The increased correlations is a consequence of an intuitively obvious fact that superconductivity is most likely to exist in valleys of minimal values of  $\mathcal{V}_i$ . For weakly correlated disorder, superconductive clusters, determined by the BCS coherence length  $\xi$ , are much larger than disorder potential textures, determined by  $\xi_{\mathcal{V}}$ , reducing correlations between the order parameter and disorder potential. However, when disorder is strongly correlated, sizes of the clusters and textures are comparable and the correlation increases.

This visual analysis of results in Fig. 1 demonstrates two opposite tendencies. A strong disorder with larger  $\mathcal{V}$  suppresses superconductivity, which is accompanied by the increased inhomogeneity and clusterization with the larger area of N islands. In contrast, a larger degree of correlation  $\alpha$  enhances superconductivity and smears out the clusters giving rise to a more homogeneous profile.

**Order parameter distribution.** Statistical properties of the order parameter  $\Delta_i$  are visualized by its absolute value distribution, shown in Fig. 3a–c for a few values of  $\mathcal{V}$  and  $\alpha$ . The distribution is plotted as a function of the relative order parameter  $\Delta/\bar{\Delta}$  where  $\bar{\Delta} = \overline{|\Delta_i|}$  is the averaged order parameter. In a superconductor with uncorrelated disorder, this distribution is well described by the log-normal function<sup>11,12,27,50</sup>

$$P(\Delta) = \frac{\bar{\Delta}}{\Delta \sqrt{2\pi\sigma}} \exp\left\{-\frac{1}{2\sigma^2} [\ln(\Delta/\bar{\Delta}) - \lambda]^2\right\}, \quad (3)$$

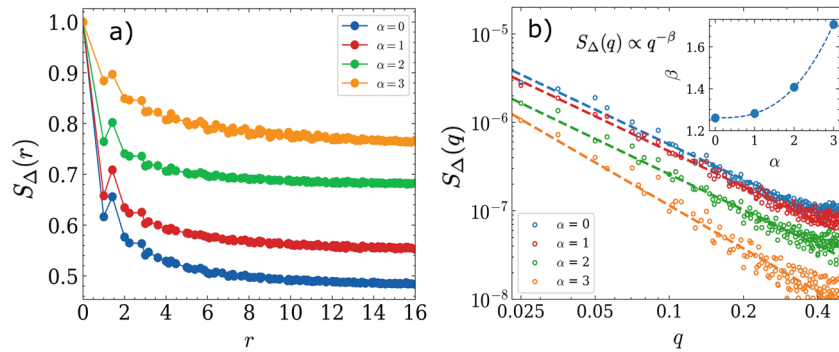


**Fig. 4 Correlation function of the order parameter.** **a** Spatial correlations of the order parameter  $S_{\Delta}(r)$ , defined in Eq. (4), calculated for several values of  $\alpha$  at  $\mathcal{V} = 1.0$ . **b** The Fourier transform  $S_{\Delta}(q)$  of the correlation function  $S_{\Delta}(r)$ , plotted in the log-log scale. The slope of its linear fit at small  $q$  (dashed lines) yields the power exponent  $\beta$  in the limiting expression  $S_{\Delta}(q) \propto q^{-\beta}$ . The inset shows the power exponent  $\beta$  as a function of  $\alpha$ . The lines connecting numerically obtained points serve as guides for an eye.

where  $\sigma$  and  $\lambda$  are constants, regarded as fitting parameters. Dashed lines in Fig. 3a–c show the best fit using Eq. (3).

At  $\alpha = 0$  Eq. (3) yields an excellent fit for all values of  $\mathcal{V}$ . For weak disorder with  $\mathcal{V} = 1$  [blue line in Fig. 3a],  $P(\Delta)$  is maximal at  $\Delta \simeq 0.5\bar{\Delta}$ . In the limit  $\Delta/\bar{\Delta} \rightarrow 0$ , the distribution  $P(\Delta)$  approaches zero [Fig. 3a] which implies the absence of N domains. When the disorder amplitude increases to  $\mathcal{V} = 1.5$ , the maximum of the distribution shifts to smaller values of  $\Delta$  [Fig. 3b], approaching the limit  $\Delta \rightarrow 0$ . This corresponds to profiles in Fig. 1, obtained at  $\mathcal{V} = 1.5$  and  $\alpha = 0$ , where N-state clusters appear.

The distribution changes itself when the disorder is correlated and  $\alpha \neq 0$ . In the weak disorder in Fig. 3a, the distribution is still well approximated by Eq. (3) for all considered values of  $\alpha$ . The maximum is, however, shifted to larger  $\Delta$  reflecting the already noted trend [Fig. 1] that increasing disorder correlations and amplitude act in the opposite directions. This trend can be seen also for strong disorder. Figure 3b, c demonstrate the maximum is shifted to larger  $\Delta/\bar{\Delta}$  when  $\alpha$  increases.

However, when the disorder has large correlations and is strong, i.e., both  $\alpha$  and  $\mathcal{V}$  are large,  $P(\Delta)$  deviates from the log-normal form (3) at small  $\Delta$ . For  $\alpha = 3$ , the deviation is visible at  $\mathcal{V} = 1.5$  [Fig. 3b], while at  $\mathcal{V} = 2$  it is clearly seen also for  $\alpha = 2$  [Fig. 3c and the inset]. Notice that for large  $\alpha$  and  $\mathcal{V}$ ,  $P(\Delta)$  deviates qualitatively from Eq. (3). It approaches a finite value in the limit  $\Delta \rightarrow 0$  and have the opposite slope comparison to the log-normal distribution.

The changes in the distribution  $P(\Delta)$  with  $\mathcal{V}$  and  $\alpha$  are quantitatively characterized by calculating the width  $\sigma$  and  $\Delta_{\max}$  position of its peak, shown in Fig. 3d and e, respectively, as functions of  $\alpha$  at several values of  $\mathcal{V}$ . The results reveal the same opposite trends. The width  $\sigma$  increases at larger  $\mathcal{V}$  and decreases at larger  $\alpha$ , and the peak position  $\Delta_{\max}$  decreases at large  $\mathcal{V}$  and increases at large  $\alpha$ . Finally, Fig. 3f illustrates the superconductivity suppression and the appearance of N-state clusters in the order parameter profile by plotting the probability to have (close to) zero order parameter  $P(\Delta \rightarrow 0)$  (here we use the criterion  $\Delta < 0.1\bar{\Delta}$ ). The figure shows this probability increases with raising  $\mathcal{V}$  and decreases when  $\alpha$  increases.

This analysis of the order parameter distribution and its defining characteristics quantify visual changes seen in the order parameter profile in Fig. 1.

**Superconductive correlations.** We now turn to spatial correlations of the order parameter. As mentioned in the introduction a weakly disordered system is naturally characterized by the competition between the BCS coherence length and the disorder

correlation length. However, for the strong disorder the superconducting state clusterizes becoming inhomogeneous. In this case, the system is characterized by spatial correlations of the order parameter with the correlation function defined as

$$S_{\Delta}(\mathbf{r}_i, \mathbf{r}_j) = \langle \Delta_i^* \Delta_j \rangle_s = \sum_{nm} \left\langle u_i^{(m)*} u_j^{(n)} v_i^{(m)*} v_j^{(n)} \right\rangle_s, \quad (4)$$

where  $u_i^{(n)}$  and  $v_i^{(n)}$  are eigenfunctions of the HF-BdG Hamiltonian. This function describes correlations on the longer scale. In a homogeneous superconductor state it becomes constant equal to  $|\bar{\Delta}|^2$  at large distances, reflecting the off-diagonal long-range order<sup>51</sup> in the mean-field approximation. The disorder destroys the long-range order and the global superconducting correlations. The corresponding characteristic length is found as

$$\xi_{\Delta}^2 = \frac{\sum_{i,j} S_{\Delta}(\mathbf{r}_i, \mathbf{r}_j) (\mathbf{r}_i - \mathbf{r}_j)^2}{\sum_{i,j} S_{\Delta}(\mathbf{r}_i, \mathbf{r}_j)}. \quad (5)$$

In a clustered superconducting state in a disordered sample  $\xi_{\Delta}$  can be interpreted as a measure of correlations between different clusters. It differs from the much shorter BCS coherence length, which defines the superconducting pairing scale, associated with the correlation function

$$S(\mathbf{r}_i, \mathbf{r}_j) = \left\langle \left| \sum_n u_i^{(n)} v_j^{(n)} \right|^2 \right\rangle_s = \sum_{nm} \left\langle u_i^{(m)*} u_i^{(n)} v_j^{(m)*} v_j^{(n)} \right\rangle_s, \quad (6)$$

which has a meaning of a squared absolute value of the Cooper pair wave function  $|\Psi(i, j)|^2$ , averaged over disorder realizations. The BCS coherence length  $\xi$  is calculated substituting this expression in place of  $S_{\Delta}$  in Eq. (5)<sup>27</sup>. For a clean system this expression yields a standard result for the BCS coherence length  $\xi_0$ . For a dirty superconductor with uncorrelated disorder this expression gives a result close to the perturbation theory [see Supplementary Note 3].

The spatial dependence of  $S_{\Delta}(r)$ , calculated at  $\mathcal{V} = 1$  for several values of  $\alpha$ , is illustrated in Fig. 4a. As expected, the correlation drops at large distances due to disorder. However, it saturates at large distances leaving a residual correlation across the entire sample. The value of this residue increases notably with raising degree of the disorder correlation  $\alpha$ .

A quantitative measure of the long-range correlations described by  $S_{\Delta}(r)$  can be extracted from the small- $q$  asymptotic of its Fourier transform. It is shown in Fig. 4b in the log-log scale. At  $q \rightarrow 0$ , it gives a linear dependence, so that its asymptotic is also the power law  $S_{\Delta}(q) \propto q^{-\beta}$ . By fitting the linear dependence we obtain the power exponent  $\beta$  as a function of  $\alpha$ , which is shown in the inset in Fig. 4b.  $\beta$  is small when  $\alpha \lesssim 1$ , but it rises sharply at  $\alpha \gtrsim 2$ . The rising  $\beta$  means that the long-range

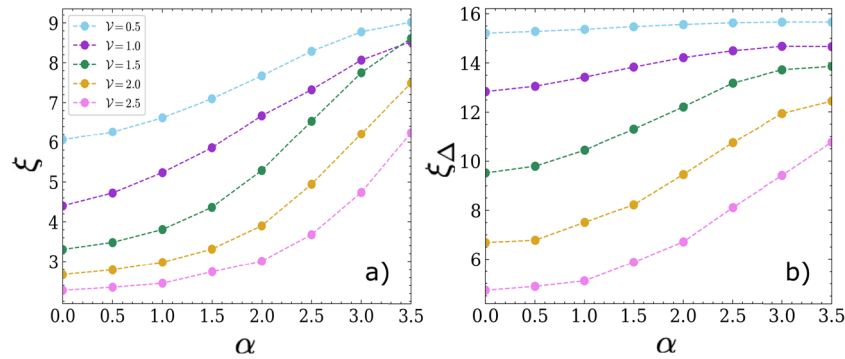


**Fig. 5 Correlation lengths.** **a** The BCS coherence length  $\xi$ . **b** The correlation length  $\xi_{\Delta}$ . Both quantities are calculated for a few selected values of  $\mathcal{V}$  and are shown as functions of  $\alpha$ . The dashed lines connecting numerically obtained points serve as guides for an eye.

superconducting correlations grow rapidly with the correlations in the disordered potential. In principle, this is consistent with the assumption that  $\alpha = 2$  is the border value separating two different regimes in the chosen model for disorder correlations. The numerical dependence is well fitted by the expression  $\beta = \beta_0 + (\alpha/4)^\gamma$  with  $\beta_0 = 1.25$  and  $\gamma = 2.75$ .

Correlation lengths  $\xi$  and  $\xi_{\Delta}$  in Fig. 5 illustrate their dependence on  $\mathcal{V}$  and  $\alpha$ . Comparing them with Fig. 2a confirms the expected relation  $\xi_{\mathcal{V}} < \xi < \xi_{\Delta}$ , which holds for all considered parameters. For uncorrelated vanishingly small disorder  $\mathcal{V} \rightarrow 0$ ,  $\xi$  yields its clean system limit ( $\sigma_0 \approx 9$ ), whereas  $\xi_{\Delta}$  approaches the effective sample dimension which is  $L/\sqrt{6} \simeq 16$ . When  $\mathcal{V}$  increases, both  $\xi$  and  $\xi_{\Delta}$  reduce monotonically. The rising correlation degree  $\alpha$  results in the opposite trend making both lengths monotonically increase. Here too, the disorder strength and correlation degree act on the correlation lengths in the opposite way.

**Superfluid stiffness.** In a strongly disordered material, the definition of superconductivity using characteristics of the local microscopic state is inadequate. In a weakly disordered sample the advance of superconductivity is unequivocally connected to the non-zero order parameter. However, in the case of strong disorder the superconductive state is strongly non-homogeneous [Fig. 1] forming weakly connected superconductive clusters with randomized phases, and the definition of superconductivity via the local or average order parameter is no longer possible. The onset of superconductivity in a finite strongly disordered sample can be characterized by the (Meissner) superfluid stiffness  $D_s^0$ <sup>52,53</sup>, which is a coefficient in the expression for the “phase rigidity” term in the energy of the superconducting condensate

$$E[\theta] = \frac{D_s^0}{2} \int d\mathbf{r} |\nabla\theta|^2, \quad (7)$$

where  $\theta$  is the phase of the superconducting order parameter. From the macroscopic point of view this is an elastic energy associated with the twisted phase of the superconductive condensate. A non-zero stiffness  $D_s^0$  means a spatial variation of the phase requires additional energy and thus the phase is rigidly fixed (“stiff”). It is the rigidity of this phase that endows a superconductor with the ability to sustain a super-current.

Within the mean-field theory the stiffness is determined by the linear response to an externally applied static vector potential<sup>52</sup>,

$$D_s^0 = -\Lambda_{xx}(q_x = 0, q_y \rightarrow 0, \omega = 0) + \langle -K_x \rangle, \quad (8)$$

where  $\Lambda_{xx}$  is the long wavelength limit of the transverse current-current correlator averaged over both the superconductive state

and the disorder realizations,

$$\Lambda_{xx}(\mathbf{q}, \omega) = \frac{1}{N} \int_0^\infty d\tau e^{i\omega\tau} \langle j_x(\mathbf{q}, \tau) j_x(-\mathbf{q}, 0) \rangle \quad (9)$$

with  $j_x(\mathbf{q}, \tau)$  being the paramagnetic current and the diamagnetic component  $\langle -K_x \rangle$  is the disorder-averaged kinetic energy along the  $x$  direction. The calculation equations for  $D_s^0$  within the BdG approach are presented in the Supplementary Note 2.

The mean-field theory calculations can be further improved by taking into account phase fluctuations within the effective XY model and the self-consistent Harmonic approximation. This gives the renormalized stiffness as<sup>12</sup>

$$D_s = D_s^0 e^{-\langle \theta_{ij}^2 \rangle_0 / 2}, \quad (10)$$

where the mean square fluctuation of the nearest neighbor phase difference is obtained as

$$\langle \theta_{ij}^2 \rangle_0 = \frac{2}{N\xi} \sum_{q < \pi} \left( \frac{\epsilon_q}{D_s \kappa} \right)^{\frac{1}{2}}, \quad (11)$$

with  $\kappa$  being the mean-field compressibility  $\kappa = dn/d\mu$  and  $\epsilon_q = 2[2 - \cos(q_x) - \cos(q_y)]$  the single-particle spectrum. Figure 6a plots the stiffness as a function of the disorder strength  $\mathcal{V}$  for a few values of correlation  $\alpha$ . The figure gives both full  $D_s$  (full circles) and the mean-field result  $D_s^0$  (open circles) for comparison. As is expected intuitively, the fluctuations reduce the stiffness and suppress superconductivity. Notice, that Eq. (11) does not account for all contributions of the quantum fluctuations. However, the role of the fluctuations is expected to decrease when the disorder becomes correlated and  $\alpha$  grows [see detailed calculations in Supplementary Note 4]. This implies that the approximate result in Eq. (11) is sufficient to qualitatively describe the  $\alpha$ -dependence of the stiffness.

In agreement with previous works<sup>12,27,54</sup> for the non-correlated disorder ( $\alpha = 0$ ), the stiffness declines when the disorder strength  $\mathcal{V}$  grows [Fig. 6a]. Here we obtain the similar dependence also for correlated disorder ( $\alpha \neq 0$ ). However, increasing correlation degree  $\alpha$  results in the larger stiffness with a consequence that the critical disorder strength, where the stiffness becomes zero, increases at larger  $\alpha$ .

It must be noted, the calculation of stiffness shows the global superconductivity ceases at much smaller values of  $\mathcal{V}$  than anticipated from the order parameter profile and its distribution. For example, the stiffness becomes zero at  $\mathcal{V} \gtrsim 0.75$  at  $\alpha = 0$ . In contrast, the order parameter is non-zero in almost the entire sample at  $\mathcal{V} = 1.0$  and  $\alpha = 0$  [Fig. 1]. It is further confirmed by the distribution  $P(\Delta)$  [Fig. 3a] and its value at  $\Delta \approx 0$  [Fig. 3f], both showing the order parameter is zero practically nowhere in the

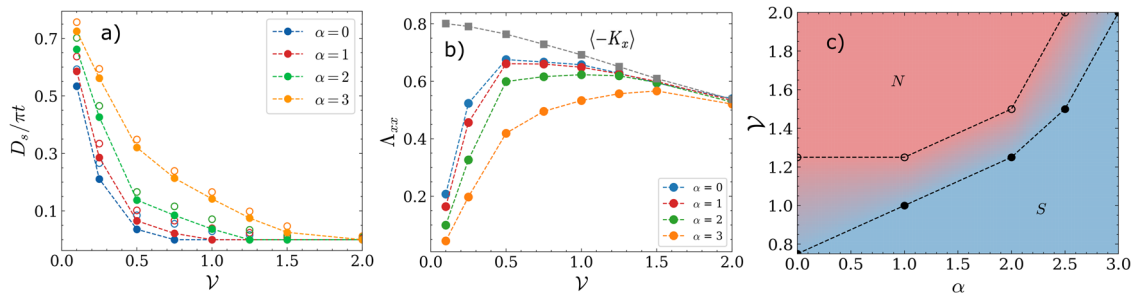


**Fig. 6 Superfluid stiffness and the phase diagram.** **a** superfluid stiffness  $D_s$  (solid circles) as a function of  $\mathcal{V}$ , calculated for selected values of  $\alpha$ . The bare BCS stiffness  $D_s^0$  is shown by open circles for comparison. **b** Diamagnetic  $\langle -K_x \rangle$  and paramagnetic  $\Lambda_{xx}(q_x = 0, q_y = 0, i\omega = 0)$  contributions to  $D_s^0$  are plotted as functions of  $\mathcal{V}$  for several values of  $\alpha$ . **c** The phase diagram of disordered superconductors in the plane  $\alpha - \mathcal{V}$ . The blue S and red N regions denote the domains of non-zero and zero stiffness, respectively. Two crossover boundaries between the S and N domains are found using the fluctuation-corrected  $D_s$  (filled circles) and bare  $D_s^0$  (empty circles) superfluid stiffness. The lines connecting the points are guides for an eye.

sample. One sees, globally non-zero order parameter is not sufficient to ensure global superconductivity.

The relations between the increased stiffness and larger disorder correlation are also traced when looking at the distribution in Fig. 3a–c. The stiffness is known to decrease due to phase twists at places where it costs less energy, i.e. where the order parameter and the condensate density  $n_s$  are minimal. When the correlation degree  $\alpha$  increases, the distributions in Fig. 3a–c shift towards larger  $\Delta$ 's, leading to the larger stiffness.

It is worth to consider diamagnetic  $\langle -K_x \rangle$  and paramagnetic  $\Lambda_{xx}$  contributions to the stiffness separately [Fig. 6b].  $\langle -K_x \rangle$  is a slowly decreasing function of  $\mathcal{V}$ . It does not depend on  $\alpha$  because it is proportional to the total electron density  $n_e$ .

The paramagnetic contribution  $\Lambda_{xx}$  behaves differently. For the clean system with  $\mathcal{V} = 0$ , the total current in the system is proportional to its momentum. Therefore, the respective current operator commutes with the Hamiltonian and the current-current correlator contributing to  $\Lambda_{xx}(q_x = 0, q_y \rightarrow 0, \omega = 0)$  vanishes. In a disordered system, the operator of the total current no longer commutes with the Hamiltonian, and  $\Lambda_{xx} \neq 0$ . The value of  $\Lambda_{xx}$  depends on the degree of the non-commutativity between the current and Hamiltonian operators, controlled by disorder strength and correlations [Fig. 6b].

A summary of the stiffness calculations is presented in Fig. 6c as a phase diagram in the  $\alpha - \mathcal{V}$  plane. The region of non-zero stiffness is marked by blue (S), and the region of zero-stiffness is denoted by red (N). Solid and open points are obtained using the fluctuation corrected ( $D_s$ ) and bare ( $D_s^0$ ) stiffness.

The phase diagram in Fig. 6c highlights a general tendency: the correlations inhibit the destructive influence of disorder on superconductivity. The dashed lines, connecting the points, serve as guides to an eye, but are expected to follow the real crossover lines, separating S and N domains, closely. Notice, they increase monotonically with rising  $\alpha$ . Their slope increases at  $\alpha \gtrsim 2$ , the special value for the model.

## Conclusions

This work studies superconductivity in systems with spatially correlated disorder, by solving a full set of microscopic HF-BdG equations for a finite 2D sample. The long-range correlations of the disordered potential are taken into account using the model where the Fourier components of the potential have random phases. Only the case of zero temperature is considered.

The calculations reveal a very notable role the disorder correlations play in shaping superconductivity, affecting its properties both on the local and global scales. It was shown that the superconductivity is enhanced by increasing the degree of disorder correlations. It is manifested in the changed character of

spatial profile, statistical distribution and spatial correlations of the order parameter. The statistical distribution demonstrate that multifractal features of the HF-BdG eigenstates, reported earlier for uncorrelated disorder, hold also when the disorder becomes correlated.

The correlations in the disorder potential enlarge both the BCS pairing correlations and the spatial correlations of the order parameter. The sizes and configuration of clusters in the inhomogeneous superconducting state are shown to depend strongly on the correlations degree. The global superconductivity of the sample, quantified by the superfluid stiffness, is also boosted by the disorder correlations.

Although our results are obtained for a relatively simple model of a non-structured disorder, they clearly demonstrate that spatial correlations in the disorder potential are a very important factor affecting superconductivity. It can change the whole range of superconductive properties and cannot be ignored when discussing the disorder-related effects in such materials. It is also clear, that deliberate manipulations of the disorder correlations, when possible, can be used to manipulate superconducting characteristics. This adds another design parameter to create superconductors with desired functional properties.

## Methods

**Microscopic equations for superconductivity.** To describe superconductivity with the  $s$ -wave coupling we employ the BCS Hamiltonian for the tight-binding model for the single-particle states

$$\hat{H} = \sum_{i,j,\sigma} t_{ij} \hat{c}_{i\sigma}^\dagger \hat{c}_{j\sigma} + \sum_{i,\sigma} V_i \hat{n}_{i\sigma} - g \sum_{i,\sigma} \hat{n}_{i\uparrow} \hat{n}_{i\downarrow}, \quad (12)$$

where  $\hat{c}_i$  denotes the electron operator at site  $i$  of the lattice,  $t_{ij}$  is the tunneling amplitude between sites  $i$  and  $j$  assumed non-zero  $t_{ij} = -t$  only for the nearest neighbors,  $g > 0$  is the on-site BCS coupling constant, and  $V_i$  is the impurity potential. Here we consider a 2D lattice with the vector indices denoting sites  $i = (i_x, i_y)$ . The mean field Bogoliubov – de Gennes (BdG) equations for the Hamiltonian (12) write as

$$\begin{pmatrix} \hat{H} - \mu & \hat{\Delta} \\ \hat{\Delta}^\dagger & -\hat{H}^\dagger + \mu \end{pmatrix} \begin{pmatrix} \vec{u} \\ \vec{v} \end{pmatrix} = E \begin{pmatrix} \vec{u} \\ \vec{v} \end{pmatrix}, \quad (13)$$

where  $\mu$  is the system chemical potential,  $\vec{u}$  and  $\vec{v}$  are vectors with components  $v_i$  and  $u_i$ , the operators  $\hat{H}$  and  $\hat{\Delta}$  are defined by their matrix elements

$$H_{ij} = t_{ij} + (V_i + U_i) \delta_{ij}, \quad \Delta_{ij} = \Delta_i \delta_{ij}, \quad (14)$$

with  $\delta_{ij}$  being the Kronecker symbol. The order parameter  $\Delta_i$  and Hartree potential  $U_i$  are found from the self-consistency equations

$$\Delta_i = g \langle \hat{c}_{i\downarrow} \hat{c}_{i\uparrow} \rangle, \quad (15a)$$

$$U_i = -\frac{g}{2} \sum_{\sigma} \langle \hat{c}_{i\sigma}^\dagger \hat{c}_{i\sigma} \rangle, \quad (15b)$$

where  $\langle \dots \rangle$  are quantum mechanical averages. Notice that the Hartree self-consistency Eq. (15b) modifies the effective potential for electrons in an inhomogeneous system. It plays a crucial role when the disorder is strong and cannot be

neglected as in weakly disordered systems<sup>55</sup>. The model neglects the long-range repulsive Coulomb interactions between electrons, as is also done in many previous studies of the role of disorder in superconductive systems<sup>26,27</sup>. Although the influence of the interactions can become notable in disordered systems with localized carriers, it is expected to decrease when the disorder becomes correlated. We also do not consider the  $d$ -wave pairing that can be strongly enhanced by combining the Coulomb repulsion with a fully random potential for electrons<sup>56</sup>.

**Correlated disorder model.** Disordered models with the power-law correlation asymptotic have long been proposed<sup>57</sup>, in particular, to investigate the correlation-induced changes in the Anderson localization<sup>58,59</sup>, and the percolation threshold<sup>60</sup>. Those models, sometimes referred to as *speckle*, have been applied to model, e.g., of cold gases in randomized optical lattices<sup>38,59,61–63</sup>. The power-law correlations in a spatial distribution of linear or planar crystal dislocations have been recently confirmed experimentally<sup>64</sup>, and the asymptotic (1) agreed well with those observations.

The power-law dependence (1) is realized by assuming a model with the random potential  $V_i$  on a lattice site  $i$  given by

$$V_i = \frac{1}{N^2} \sum_{j_x, j_y=1}^{N/2} q_j^{-\alpha/2} \cos(\mathbf{q}_j \mathbf{r}_i + \phi_j), \quad (16)$$

where  $\mathbf{r}_i$  is the lattice position,  $\mathbf{q}_j = (2\pi j_x/N, 2\pi j_y/N)$  is a discrete inverse space vector,  $j_{x,y} = 1, \dots, N$  and  $q_j = |\mathbf{q}_j|$ . Finally,  $\phi_j$  are random phases, uniformly distributed in the interval  $[0, 2\pi)$ . The spatial correlations of the random potential are defined as

$$S_V(\mathbf{r}_i, \mathbf{r}_j) = \langle V_i V_j \rangle_s \quad (17)$$

with brackets  $\langle \dots \rangle_s$  denoting the statistical ensemble average. Notice, that for the large system this quantity depends only on the difference  $\mathbf{r}_i - \mathbf{r}_j$ , but this is violated in practical calculations for a finite system with a limited number of disorder potential realizations. In the inverse space this correlator is obtained by evaluating a sum

$$S_V(\mathbf{q}) = \frac{1}{N^4} \sum_{ij} S_V(\mathbf{r}_i, \mathbf{r}_j) e^{i\mathbf{q}(\mathbf{r}_i - \mathbf{r}_j)}. \quad (18)$$

One can easily see the model (16) yields Eq. (1) [see Supplementary Note 1]. The dependence of  $S_V(\mathbf{q})$  calculated using numerically ensemble averages  $\langle V_i V_j \rangle_s$  of randomly generated  $V_i$  according to the model in Eq. (16) is shown in Fig. 2b for a few selected values of  $\alpha$  ( $S_V(\mathbf{q})$  depends only on  $q$  for a homogeneous system). For all values of  $\alpha$ , the log-log dependence is linear with the slope  $-\alpha$  in full agreement with Eq. (1). Notice, that  $V_q \propto \sqrt{S_V(\mathbf{q})}$ , where  $V_q$  is the Fourier transform of the potential defined in Eq. (16) but without the random phases.

Spatial correlations in the real space can be characterized by the correlation length  $\xi_V$  calculated as

$$\xi_V^2 = \frac{\sum_{ij} S_V(\mathbf{r}_i, \mathbf{r}_j) (\mathbf{r}_i - \mathbf{r}_j)^2}{\sum_{ij} S_V(\mathbf{r}_i, \mathbf{r}_j)}. \quad (19)$$

The calculated  $\xi_V$  is shown in Fig. 2a. It increases monotonically as a function of  $\alpha$ , indicating a larger correlation length at larger  $\alpha$ . At  $\alpha = 0$  this length is  $\xi < 1$ , meaning the potential is fully uncorrelated at the most close lattice sites.

Finally, it is convenient to shift the potential as

$$V_i \rightarrow V_i - \bar{V}_i, \quad \bar{V}_i = \sum_i \langle V_i \rangle_s \quad (20)$$

to ensure its average value is zero. Here the numerical averaging denoted by the overline is done both over lattice sites and the statistical distribution. This constant shift in the potential excludes the change in the chemical potential. The amplitude of the disorder potential is defined by the quantity

$$\mathcal{V} = \sqrt{\bar{V}_i^2}, \quad (21)$$

referred to as *disorder strength*.

The model in Eq. (16) was employed to describe real stochastic processes with the long-range correlations including nucleotide sequences in DNA molecules<sup>65,66</sup>, and other systems where disorder correlations affects electronic transport, plasma fluctuations<sup>67</sup>, and patterns in surface growth<sup>68</sup>.

**Numerical parameters.** Equations (13) are solved numerically on a square lattice with dimensions  $A = N \times N$  with the periodic boundary conditions. We take  $N = 40$  which is an optimal trade-off between the numerical load and our goal to describe a bulk system, where results are already not sensitive to the sample size. The chemical potential  $\mu$  is chosen so that the average electron density is set to  $n_e = 0.875$ . We note that a particular value of  $n_e$  is not important for as long as we sufficiently far from the half filling of  $n_e = 1$  with additional symmetries.

The analysis is done in the limit of nominally large coupling constant of  $g = 1$ , and the limit of very large Debye window of  $\hbar\omega_D = 5$ , which implied the coupling involves all single-particle states. (All energy quantities in the problem are expressed in units of the hopping integral  $t$ .) Note, however, that a typical average value of the gap function  $\bar{\Delta} \simeq 0.04$  is much less than the Fermi energy  $E_F \simeq 3.76$ .

The ratio of the two quantities  $\bar{\Delta}/E_F \simeq 0.01$ , which implies that we are in the weak coupling regime of BCS superconductivity. Finally, the physical quantities of interest are statistically averaged over  $N_s = 50$  independent disorder realizations that has the same  $\mathcal{V}$  and  $\alpha$ .

## Data availability

The data-sets generated during and/or analyzed during the current study are available from the corresponding author on reasonable request.

Received: 11 December 2021; Accepted: 31 May 2022;

Published online: 06 July 2022

## References

1. Abrikosov, A. & Gor'kov, L. Superconducting alloys at finite temperatures. *J. Exp. Theor. Phys.* **36**, 220 (1959).
2. Anderson, P. Theory of dirty superconductors. *J. Phys. Chem. Solids* **11**, 26–30 (1959).
3. Goldman, A. M. & Marković, N. Superconductor-insulator transitions in the two-dimensional limit. *Phys. Today* **51**, 39–44 (1998).
4. Gantmakher, V. F. & Dolgoplov, V. T. Superconductor-insulator quantum phase transition. *Phys. Usp.* **180**, 3 (2010).
5. Sadoyskii, M. V. Superconductivity and localization. *Phys. Rep.* **282**, 225–348 (1997).
6. Shahar, D. & Ovadyahu, Z. Superconductivity near the mobility edge. *Phys. Rev. B* **46**, 10917–10922 (1992).
7. Sambandamurthy, G., Engel, L. W., Johansson, A., Peled, E. & Shahar, D. Experimental evidence for a collective insulating state in two-dimensional superconductors. *Phys. Rev. Lett.* **94**, 017003 (2005).
8. Steiner, M. A., Breznay, N. P. & Kapitulnik, A. Approach to a superconductor-to-bose-insulator transition in disordered films. *Phys. Rev. B* **77**, 212501 (2008).
9. Sacépé, B. et al. Pseudogap in a thin film of a conventional superconductor. *Nat. Commun.* **1**, 140 (2010).
10. Sacépé, B. et al. Disorder-induced inhomogeneities of the superconducting state close to the superconductor-insulator transition. *Phys. Rev. Lett.* **101**, 157006 (2008).
11. Ghosal, A., Randeria, M. & Trivedi, N. Role of spatial amplitude fluctuations in highly disordered  $s$ -wave superconductors. *Phys. Rev. Lett.* **81**, 3940–3943 (1998).
12. Ghosal, A., Randeria, M. & Trivedi, N. Inhomogeneous pairing in highly disordered  $s$ -wave superconductors. *Phys. Rev. B* **65**, 014501 (2001).
13. Dubi, Y., Meir, Y. & Avishai, Y. Nature of the superconductor-insulator transition in disordered superconductors. *Nature* **449**, 876–880 (2007).
14. Brun, C. et al. Remarkable effects of disorder on superconductivity of single atomic layers of lead on silicon. *Nat. Phys.* **10**, 444–450 (2014).
15. Lemarié, G. et al. Universal scaling of the order-parameter distribution in strongly disordered superconductors. *Phys. Rev. B* **87**, 184509 (2013).
16. Noat, Y. et al. Unconventional superconductivity in ultrathin superconducting NbN films studied by scanning tunneling spectroscopy. *Phys. Rev. B* **88**, 014503 (2013).
17. Mondal, M. et al. Phase fluctuations in a strongly disordered  $s$ -wave NbN superconductor close to the metal-insulator transition. *Phys. Rev. Lett.* **106**, 047001 (2011).
18. Mondal, M. et al. Enhancement of the finite-frequency superfluid response in the pseudogap regime of strongly disordered superconducting films. *Sci. Rep.* **3**, 1357 (2013).
19. Saito, Y., Nojima, T. & Iwasa, Y. Highly crystalline 2d superconductors. *Nat. Rev. Mater.* **2**, 16094 (2016).
20. Arrighoni, E. & Kivelson, S. A. Optimal inhomogeneity for superconductivity. *Phys. Rev. B* **68**, 180503 (2003).
21. Petrović, A. P. et al. A disorder-enhanced quasi-one-dimensional superconductor. *Nat. Commun.* **7**, 12262 (2016).
22. Peng, J. et al. Disorder enhanced superconductivity toward TaS<sub>2</sub> monolayer. *ACS Nano* **12**, 9461–9466 (2018).
23. Zhao, K. et al. Disorder-induced multifractal superconductivity in monolayer niobium dichalcogenides. *Nat. Phys.* **15**, 904–910 (2019).
24. Feigel'man, M., Ioffe, L., Kravtsov, V. & Cuevas, E. Fractal superconductivity near localization threshold. *Ann. Phys.* **325**, 1390–1478 (2010).
25. Rubio-Verdú, C. et al. Visualization of multifractal superconductivity in a two-dimensional transition metal dichalcogenide in the weak-disorder regime. *Nano Lett.* **20**, 5111–5118 (2020).
26. Gastiasoro, M. N. & Andersen, B. M. Enhancing superconductivity by disorder. *Phys. Rev. B* **98**, 184510 (2018).



27. Fan, B. & García-García, A. M. Enhanced phase-coherent multifractal two-dimensional superconductivity. *Phys. Rev. B* **101**, 104509 (2020).
28. Martin, I., Podolsky, D. & Kivelson, S. A. Enhancement of superconductivity by local inhomogeneities. *Phys. Rev. B* **72**, 060502 (2005).
29. Croitoru, M. D., Shanenko, A. A., Kaun, C. C. & Peeters, F. M. Metallic nanograins: Spatially nonuniform pairing induced by quantum confinement. *Phys. Rev. B* **83**, 214509 (2011).
30. Croitoru, M. D. et al. Phonon limited superconducting correlations in metallic nanograins. *Sci. Rep.* **5**, 16515 (2015).
31. Croitoru, M. D. et al. Influence of disorder on superconducting correlations in nanoparticles. *J. Superconductivity Nov. Magn.* **29**, 605–609 (2016).
32. Keen, D. A. & Goodwin, A. L. The crystallography of correlated disorder. *Nature* **521**, 303–309 (2015).
33. Simonov, A. & Goodwin, A. L. Designing disorder into crystalline materials. *Nat. Rev. Chem.* **4**, 657–673 (2020).
34. Damasceno, P. F., Engel, M. & Glotzer, S. C. Predictive self-assembly of polyhedra into complex structures. *Science* **337**, 453–457 (2012).
35. Krokhin, A. A., Bagci, V. M. K., Izrailev, F. M., Usatenko, O. V. & Yampol'skii, V. A. Inhomogeneous DNA: Conducting exons and insulating introns. *Phys. Rev. B* **80**, 085420 (2009).
36. de Moura, F. A. B. F. & Lyra, M. L. Delocalization in the 1d anderson model with long-range correlated disorder. *Phys. Rev. Lett.* **81**, 3735 (1998).
37. Kuhl, U., Izrailev, F. M. & Krokhin, A. A. Enhancement of localization in one-dimensional random potentials with long-range correlations. *Phys. Rev. Lett.* **100**, 126402 (2008).
38. Billy, J. et al. Direct observation of anderson localization of matter waves in a controlled disorder. *Nature* **453**, 891–894 (2008).
39. Sanchez-Palencia, L. & Lewenstein, M. Disordered quantum gases under control. *Nat. Phys.* **6**, 87–95 (2010).
40. Dietz, O., Kuhl, U., Stöckmann, H.-J., Makarov, N. M. & Izrailev, F. M. Microwave realization of quasi-one-dimensional systems with correlated disorder. *Phys. Rev. B* **83**, 134203 (2011).
41. Chaney, D. et al. Tuneable correlated disorder in alloys. *Phys. Rev. Mater.* **5**, 035004 (2021).
42. Düvel, A. et al. Is geometric frustration-induced disorder a recipe for high ionic conductivity? *J. Am. Chem. Soc.* **139**, 5842–5848 (2017).
43. Senn, M., Keen, D., Lucas, T., Hriljac, J. & Goodwin, A. Emergence of long-range order in BaTiO<sub>3</sub> from local symmetry-breaking distortions. *Phys. Rev. Lett.* **116**, 207602 (2016).
44. Krogstad, M. J. et al. The relation of local order to material properties in relaxor ferroelectrics. *Nat. Mater.* **17**, 718–724 (2018).
45. Sangiorgio, B. et al. Correlated local dipoles in PbTe. *Phys. Rev. Mater.* **2**, 085402 (2018).
46. Weller, M. T., Weber, O. J., Henry, P. F., Pumpo, A. M. D. & Hansen, T. C. Complete structure and cation orientation in the perovskite photovoltaic methylammonium lead iodide between 100 and 352 k. *Chem. Commun.* **51**, 4180–4183 (2015).
47. Goodwin, A. L. Opportunities and challenges in understanding complex functional materials. *Nat. Commun.* **10**, 4461 (2019).
48. Kivelson, S. Making high *t<sub>c</sub>* higher: a theoretical proposal. *Phys. B: Condens. Matter* **318**, 61–67 (2002).
49. Tsai, W.-F., Yao, H., Läuchli, A. & Kivelson, S. A. Optimal inhomogeneity for superconductivity: Finite-size studies. *Phys. Rev. B* **77**, 214502 (2008).
50. Mayoh, J. & García-García, A. M. Global critical temperature in disordered superconductors with weak multifractality. *Phys. Rev. B* **92**, 174526 (2015).
51. Yang, C. N. Concept of off-diagonal long-range order and the quantum phases of liquid He and of superconductors. *Rev. Mod. Phys.* **34**, 694–704 (1962).
52. Scalapino, D. J., White, S. R. & Zhang, S. C. Superfluid density and the drude weight of the hubbard model. *Phys. Rev. Lett.* **68**, 2830–2833 (1992).
53. Scalapino, D. J., White, S. R. & Zhang, S. Insulator, metal, or superconductor: The criteria. *Phys. Rev. B* **47**, 7995–8007 (1993).
54. Chakraborty, D. & Ghosal, A. Fate of disorder-induced inhomogeneities in strongly correlated d-wave superconductors. *N. J. Phys.* **16**, 103018 (2014).
55. Tarat, S. & Majumdar, P. Charge dynamics across the disorder-driven superconductor-insulator transition. *Europhys. Lett.* **105**, 67002 (2014).
56. Römer, A. T., Hirschfeld, P. J. & Andersen, B. M. Raising the critical temperature by disorder in unconventional superconductors mediated by spin fluctuations. *Phys. Rev. Lett.* **121**, 027002 (2018).
57. Weinrib, A. & Halperin, B. I. Critical phenomena in systems with long-range-correlated quenched disorder. *Phys. Rev. B* **27**, 413–427 (1983).
58. Sanchez-Palencia, L. et al. Anderson localization of expanding bose-einstein condensates in random potentials. *Phys. Rev. Lett.* **98**, 210401 (2007).
59. Sanchez-Palencia, L. & Lewenstein, M. Disordered quantum gases under control. *Nat. Phys.* **6**, 87–95 (2010).
60. Zierenberg, J. et al. Percolation thresholds and fractal dimensions for square and cubic lattices with long-range correlated defects. *Phys. Rev. E* **96**, 062125 (2017).
61. Semmler, D., Wernsdorfer, J., Bissbort, U., Byczuk, K. & Hofstetter, W. Localization of correlated fermions in optical lattices with speckle disorder. *Phys. Rev. B* **82**, 235115 (2010).
62. Delande, D. & Orso, G. Mobility edge for cold atoms in laser speckle potentials. *Phys. Rev. Lett.* **113**, 060601 (2014).
63. Pilati, S. & Fratini, E. Ferromagnetism in a repulsive atomic fermi gas with correlated disorder. *Phys. Rev. A* **93**, 051604 (2016).
64. Choi, W., Yin, C., Hooper, I. R., Barnes, W. L. & Bertolotti, J. Absence of anderson localization in certain random lattices. *Phys. Rev. E* **96**, 022122 (2017).
65. Peng, C.-K. et al. Long-range correlations in nucleotide sequences. *Nature* **356**, 168–170 (1992).
66. Carpena, P., Bernal-Galván, P., Ivanov, P. C. & Stanley, H. E. Metal-insulator transition in chains with correlated disorder. *Nature* **418**, 955–959 (2002).
67. Carreras, B. A. et al. Long-range time correlations in plasma edge turbulence. *Phys. Rev. Lett.* **80**, 4438–4441 (1998).
68. Lam, C.-H. & Sander, L. M. Surface growth with power-law noise. *Phys. Rev. Lett.* **69**, 3338–3341 (1992).

### Acknowledgements

The authors are grateful to the Basic Research Program of the HSE University. V.D.N., A.E.L., A.V.K. acknowledge support from the Russian Foundation for Basic Research under the Project 20-21-00085. M.D.C. acknowledges the UFPE Propesq program (grant: Edital Professor Visitante-Edital Propesq nr. 05.2018), Recife-PE, Brazil. The calculations were performed using resources of NRNU MEPhI high-performance computing cluster and with the support of the MEPhI Program Priority 2030.

### Author contributions

M.D.C. initiated the idea. V.D.N. and A.E.L. performed calculations. A.V.K., A.V., and M.D.C. wrote the paper. All authors contributed to discussing the data and editing the paper.

### Competing interests

The authors declare no competing interests.

### Additional information

**Supplementary information** The online version contains supplementary material available at <https://doi.org/10.1038/s42005-022-00933-z>.

**Correspondence** and requests for materials should be addressed to Andrey V. Krasavin.

**Peer review information** *Communications Physics* thanks the anonymous reviewers for their contribution to the peer review of this work.

**Reprints and permission information** is available at <http://www.nature.com/reprints>

**Publisher's note** Springer Nature remains neutral with regard to jurisdictional claims in published maps and institutional affiliations.



**Open Access** This article is licensed under a Creative Commons Attribution 4.0 International License, which permits use, sharing, adaptation, distribution and reproduction in any medium or format, as long as you give appropriate credit to the original author(s) and the source, provide a link to the Creative Commons license, and indicate if changes were made. The images or other third party material in this article are included in the article's Creative Commons license, unless indicated otherwise in a credit line to the material. If material is not included in the article's Creative Commons license and your intended use is not permitted by statutory regulation or exceeds the permitted use, you will need to obtain permission directly from the copyright holder. To view a copy of this license, visit <http://creativecommons.org/licenses/by/4.0/>.

© The Author(s) 2022